SCIENTIFIC REPORTS
nature research

OPEN

Controlled synthesis and luminescence properties of core-shell-shell structured SiO_2@AIPA-S-Si-Eu@SiO_2 and SiO_2@AIPA-S-Si-Eu-phen@SiO_2 nanocomposites

Yan Qiao[1], Wenxian Li[1*], Jinrong Bao[1], Yushan Zheng[2], Lina Feng[1], Yangyang Ma[1], Kuisuo Yang[1], Anping Wu[1], He Bai[1] & Yunjiang Yang[1]

Two novel core-shell structured SiO_2@AIPA-S-Si-Eu and SiO_2@AIPA-S-Si-Eu-phen nanocomposites have been synthesized by a bifunctional organic ligands ($(HOOC)_2C_6H_3NHCONH(CH_2)_3Si(OCH_2CH_3)_3$) (defined as AIPA-S-Si) connected with Eu^{3+} ions and silica via covalent bond. And the corresponding core-shell-shell structured SiO_2@AIPA-S-Si-Eu@SiO_2 and SiO_2@AIPA-S-Si-Eu-phen@SiO_2 nanocomposites with enhanced luminescence have been synthesized by tetraethyl orthosilicate (TEOS) hydrolysis co-deposition method. The composition and micromorphology of the nanocomposites were characterized by means of Fourier-transform infrared spectroscopy (FT-IR), thermal gravimetric analysis (TG), X-ray diffraction (XRD), scanning electron microscopy (SEM), transmission electron microscopy (TEM), energy-dispersive X-ray spectrometry (EDX) and X-ray photoelectron spectroscopy (XPS). The as-synthesized core-shell and core-shell-shell structured nanocomposites have excellent luminescence intensity and long lifetime. The nanocomposites show bright red light under ultraviolet lamp. However, the core-shell-shell structured nanocomposites have stronger luminescence intensity than the corresponding core-shell structured nanocomposites. Meanwhile, the core-shell-shell structured nanocomposites still exhibit good luminescence stability in aqueous solution. In addition, a large number of Si-OH on the surface of the core-shell-shell structured nanocomposites can be attached to many biomacromolecules. Therefore, they have potential applications in the fields of biology and luminescence.

In recent years, core-shell structured nanocomposites are gaining increasing attention due to their unique structures and properties. Core-shell structured nanocomposites not only have core properties but also shell properties, or new properties depend on the interaction between the core and the shell. This unique property also makes it a very important emerging nanomaterial that is widely used in various fields. For example, bio-nanotechnology, optics, electroluminescence devices, bio-imaging energy storage materials, etc.[1–8].

Silica is commonly used as core and shell material in core-shell structured nanocomposites due to its high mechanical stability, low cost, low cytotoxicity, ease of preparation, and bioconpatibility[9–12]. So far, many research groups have studied core-shell structured nanocomposites using silica as core and shell, which have potential applications in different fields. Yan's group had reported the SiO_2@lanthanide complex@MOF composites with excellent properties for metal ion sensing[13]. Li's group had reported the SiO_2@Tb/GMP as fluorescence sensor probe[14]. Tobias's group had reported that SiO_2@Pt@SiO_2 is used as a new type of optical component[15]. In previous studies, our group reported that the core-shell structured nanocomposite SiO_2@MABA-Si-Tb was synthesized by using MABA-Si as a ligand. It is found that SiO_2 can improve the luminescence intensity and stability of rare earth complexes, which has potential application prospects in the field of luminescence[16].

[1]Inner Mongolia Key Laboratory of Chemistry and Physics of Rare Earth Materials, School of Chemistry and Chemical Engineering, Inner Mongolia University, Hohhot, 010021, China. [2]Inner Mongolia Autonomous Region Food Inspection Test center, Hohhot, 010021, China. *email: nmglwx@163.com

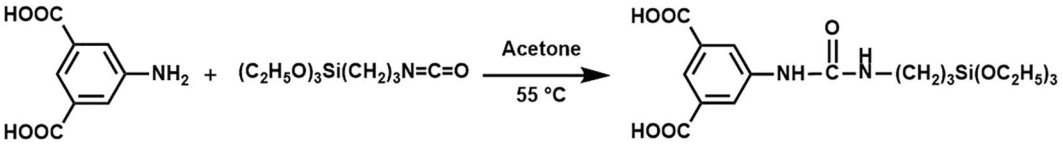

Scheme 1. The synthesis mechanism of ligand AIPA-S-Si.

Over the years, though the core-shell structured nanocomposite with silica coating inorganic materials were successive studied[17–19], but their weaker luminescent properties limit their application in many fields. However, the rare earth organic complexes have excellent luminescence properties, which the energy of the organic ligands was efficiently transferred into the rare earth ions by "antenna effect"[20]. Besides, rare earth organic complexes have strong and narrow emission bands and are widely used in many optical fields. Unfortunately, rare earth organic complex themselves are still restricted from being utilized in practical applications due to their poor thermal and mechanical stability[13]. If the rare earth organic complex were immobilized on the surface of the silica, the silica core can reduce the skeleton vibration of the ligand, thereby effectively improving the stability and luminescence intensity of the complex[21–23]. The nanocomposites with silica as the core and rare earth complexes as the shell have good luminous properties, which make them more widely used. However, in the core-shell structured nanocomposites, the rare earth organic complex of the outer shell layer being exposed to the environment, which tends to quench the luminescence. In order to overcome this problem, the core-shell structured nanocomposite is coated with an amorphous silica to form a core-shell-shell structured nanocomposite, which can improve the luminescent properties of nanocomposites. The core-shell-shell structured nanocomposites designed in this way has excellent luminescence properties and good stability. In addition, the SiO_2 shell coated on the surface of the core-shell structured nanocomposite is easily condensed with the -OH group on other molecules to form a Si-O-Si network, and various functional groups are easily introduced into the silica shell, which is widely used in biomedicine[24–26].

Up to now, there are two main methods for preparing core-shell structured nanocomposites: direct precipitation method and silane coupling agent method. Direct precipitation method is to deposit functional shell materials directly on the surface of SiO_2 core. The method is simple to operate, but the prepared nanocomposites are unstable and prone to collapse. The silane coupling method is to join the SiO_2 core and the shell by a covalent bond. What' more, the shell layer thickness of nanocomposites is easy to control and structurally stable via this method. The realization of this method is challenging. It was have a silane coupling agent called a "molecular bridge" to bond rare earth ions and SiO_2. Accordingly, it is important to choose a suitable silane coupling agent.

In this work, firstly, we synthesized the bifunctional organic ligands $((HOOC)_2C_6H_3NHCONH(CH_2)_3Si(OCH_2CH_3)_3$, it is obtained by single-substitution of hydrogen atom on the amino group of AIPA by TEPIC. Defined as AIPA-S-Si) using 5-amino-phthalic acid (AIPA) and the silane coupling agent 3-(triethoxysilyl)-propyl isocyanate (TEPIC). The as-prepared ligand (AIPA-S-Si) has two carboxyl groups, which are easier to coordinate with rare earth Eu^{3+} ions so that the synthesized nanocomposites have excellent luminescence properties. Then four kinds of nanocomposites SiO_2@AIPA-S-Si-Eu, SiO_2@AIPA-S-Si-Eu-phen, SiO_2@AIPA-S-Si-Eu@SiO_2 and SiO_2@AIPA-S-Si-Eu-phen@SiO_2 were successfully prepared by the bifunctional organic ligands (AIPA-S-Si). The luminescence spectra indicated that the as-synthesized nanocomposites have strong luminescence properties. Because SiO_2 shell can protect core-shell structured nanocomposites from the influence of external environment, the luminous efficiency of core-shell-shell structured nanocomposites are higher than that of the corresponding core-shell structured nanocomposites. The as-synthesized core-shell and core-shell-shell structured nanocomposites greatly reduce the amount of rare earth and the production cost is reduced in practical application. More importantly, many Si-OH groups on the surface of core-shell-shell structured nanocomposites can be easily connected with biomolecules, which can be widely studied in the field of biology.

Results and Discussion

Formation mechanism of core-shell and core-shell-shell structured nanocomposites. The synthesis mechanism of the ligand AIPA-S-Si was shown in Scheme 1. Specifically, the bifunctional ligand AIPA-S-Si was obtained by linking an amino group of AIPA having carboxyl group and isocyanate group of TEPIC having ethoxy group. From the structure of the ligand AIPA-S-Si, the carboxyl group on one side of the ligand is coordinated with Eu^{3+}, and the ethoxy group on the other side is connected by hydrolysis and condensation with the silanol group on the surface of the SiO_2 microspheres. The synthesis mechanism of core-shell and core-shell-shell structured nanocomposites were shown in Scheme 2. In this work, SiO_2 was a core, AIPA-S-Si was the first ligand, and phen was the second ligand. The SiO_2 was modified by hydrolysis and condensation of silanol groups on the surface of the silica microspheres and alkoxy groups on the first ligand AIPA-S-Si. A mount of carboxylic group exposed on the surface of the modified SiO_2. Then, the Eu^{3+} ions coordinated with the carboxylic oxygen atoms of ligand (AIPA-S-Si) on the surface of the modified SiO_2 and nitrogen atoms of second ligand phen. The core-shell structured nanocomposites were formed by "molecular bridge". Finally, the core-shell-shell structured nanocomposites were prepared by TEOS hydrolyzed on the surface of the core-shell structured nanocomposites under the action of CTAB.

SEM and TEM analysis of SiO_2 and SiO_2@AIPA-S-Si. The morphology and structure of all samples were further investigated by scanning and transmission electron microscopy. Figure 1(a,b) shows the SEM and TEM of SiO_2 microspheres. It can be observed that SiO_2 has smooth surface and good dispersibility with an

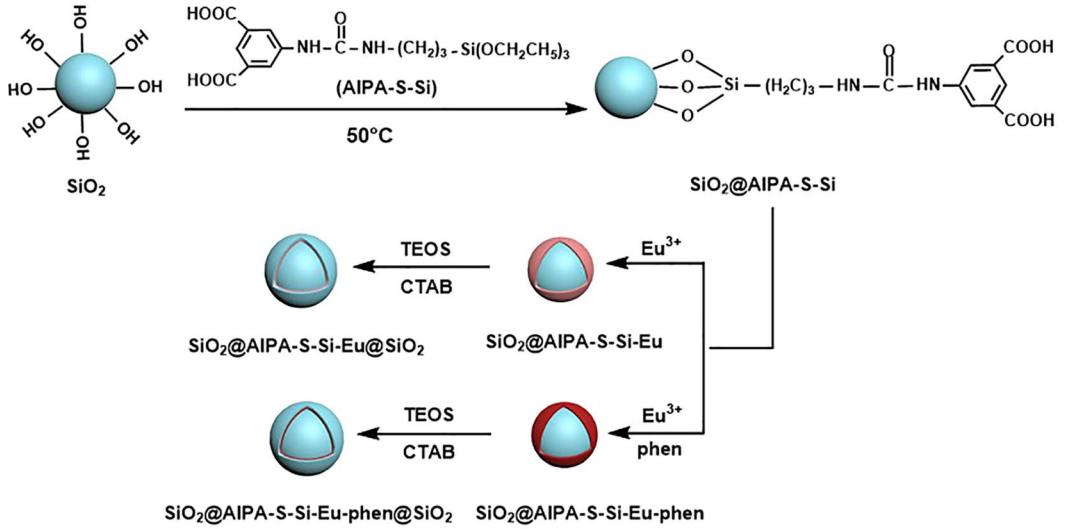

Scheme 2. The synthesis mechanism of core-shell and core-shell-shell structured nanocomposites.

average diameter of about 180 nm. SEM and TEM of SiO_2@AIPA-S-Si in Fig. 1(d,e) shows that the surface of the SiO_2 microspheres were slightly rough. Nevertheless, it was worth noting that the size distribution of Fig. 1(c,f) shows that there was a significant difference in diameter between SiO_2 and SiO_2@AIPA-S-Si, and the diameter of SiO_2@AIPA-S-Si increases by about 10 nm compared with SiO_2 microspheres. The results showed that the organic ligand was successfully grafted onto the surface of the SiO_2 microspheres.

TEM analysis of core-shell and core-shell-shell structured nanocomposites. The TEM images of SiO_2@AIPA-S-Si-Eu and SiO_2@AIPA-S-Si-Eu@SiO_2 nanocomposites were presented in Fig. 2(a,b,d,e). Accordingly, the TEM images of SiO_2@AIPA-S-Si-Eu-phen and SiO_2@AIPA-S-Si-Eu-phen@SiO_2 nanocomposites were shown in Fig. S1(a,b,d,e). It can be observed from Fig. 2(a,b) and Fig. S1(a,b) that the SiO_2@AIPA-S-Si-Eu and SiO_2@AIPA-S-Si-Eu-phen nanocomposites have a rougher surface than SiO_2@AIPA-S-Si, but still have good dispersibility. Furthermore, the surface roughness of core-shell-shell structured nanocomposites are very different from that of the corresponding core-shell structured nanocomposites. It can be seen from Figs. 2 and S1(d,e) that the gray layer was attached to the surface of the core-shell structured nanocomposites. Specifically, the amorphous silica layer approximately of 8–10 nm thick was successfully coated onto the SiO_2@AIPA-S-Si-Eu and SiO_2@AIPA-S-Si-Eu-phen, respectively. In addition, the EDX analysis that was performed on the core-shell and core-shell-shell structured nanocomposites suggested that the existence of N, O, Si, Cl and Eu peaks in the spectra (Figs. 2 and S1(c,f)). The strong peaks of Cu and C that can be observed from the spectra are due to the carbon coated copper grid. It can be found that the contents of Eu in SiO_2@AIPA-S-Si-Eu, SiO_2@AIPA-S-Si-Eu@SiO_2, SiO_2@AIPA-S-Si-Eu-phen and SiO_2@AIPA-S-Si-Eu-phen@SiO_2 nanocomposites were 3.47%, 0.17%, 4.09% and 0.22%, respectively. The content of Eu in the core-shell-shell structured nanocomposite is lower than that of the corresponding core-shell structured nanocomposite, which further proves that the amorphous silica is successfully coated on the surface of the core-shell structured nanocomposite. In addition, TEM mapping measurements of SiO_2@AIPA-S-Si-Eu@SiO_2 (Fig. 3) and SiO_2@AIPA-S-Si-Eu-phen@SiO_2 (Fig. S2) nanocomposites were performed, which exhibited uniform distributions of N, O, Si, Cl, and Eu components throughout the nanocomposites. The above data further demonstrated the successful synthesis of core-shell and core-shell-shell structured nanocomposites.

The FT-IR spectra analysis of AIPA-S-Si. The FT-IR spectra further confirmed the synthesis of ligand AIPA-S-Si. Figure S3 shows the FT-IR spectra of the AIPA (a) and AIPA-S-Si (b). For the FT-IR spectra of AIPA (a), bands located at 3425 cm^{-1} and 1695 cm^{-1} were assigned to the stretching vibration of hydroxyl (ν_{OH}) and carbonyl groups ($\nu_{C=O}$), respectively. The emergence of band located at 1629 cm^{-1} belongs to the stretching vibration of NH (ν_{N-H}). In the FT-IR spectrum of AIPA-S-Si (b), the appearance of the new bands located at around 1573 cm^{-1} and 1635 cm^{-1} due to the absorption of amide groups (–CONH–). Besides, the presence of stretching vibrations of methyl ($-CH_3$) and methylene groups ($-CH_2$) were located at 2977 cm^{-1}, 2931 cm^{-1} and 2885 cm^{-1} from TEPIC. In addition, the stretching vibration (ν_{Si-O}) located at 1103 cm^{-1} and the stretching vibration (ν_{Si-C}) located at 956 cm^{-1} suggested that TEPIC has been successfully grafted onto AIPA[27–32]. The above data indicates that the ligand AIPA-S-Si has been successfully synthesized.

The FT-IR spectra analysis of SiO_2@AIPA-S-Si-Eu and SiO_2@AIPA-S-Si-Eu@SiO_2. The FT-IR spectra was conducted to confirm the presence of chemical groups in the nanocomposites. At the same time, the synthesis of core-shell and core-shell-shell structured nanocomposites were further confirmed. The FT-IR spectra of SiO_2, SiO_2@AIPA-S-Si, SiO_2@AIPA-S-Si-Eu and SiO_2@AIPA-S-Si-Eu@SiO_2 were shown in Fig. S4. In the spectrum of SiO_2 (Fig. S4a), the characteristic absorption band of Si-O-Si located at 1095 cm^{-1} ($\nu_{Si-O-Si}$), 470 cm^{-1} ($\delta_{Si-O-Si}$) and Si-OH was identified at 956 cm^{-1} [33,34]. The characteristic absorption band of the SiO_2@AIPA-S-Si

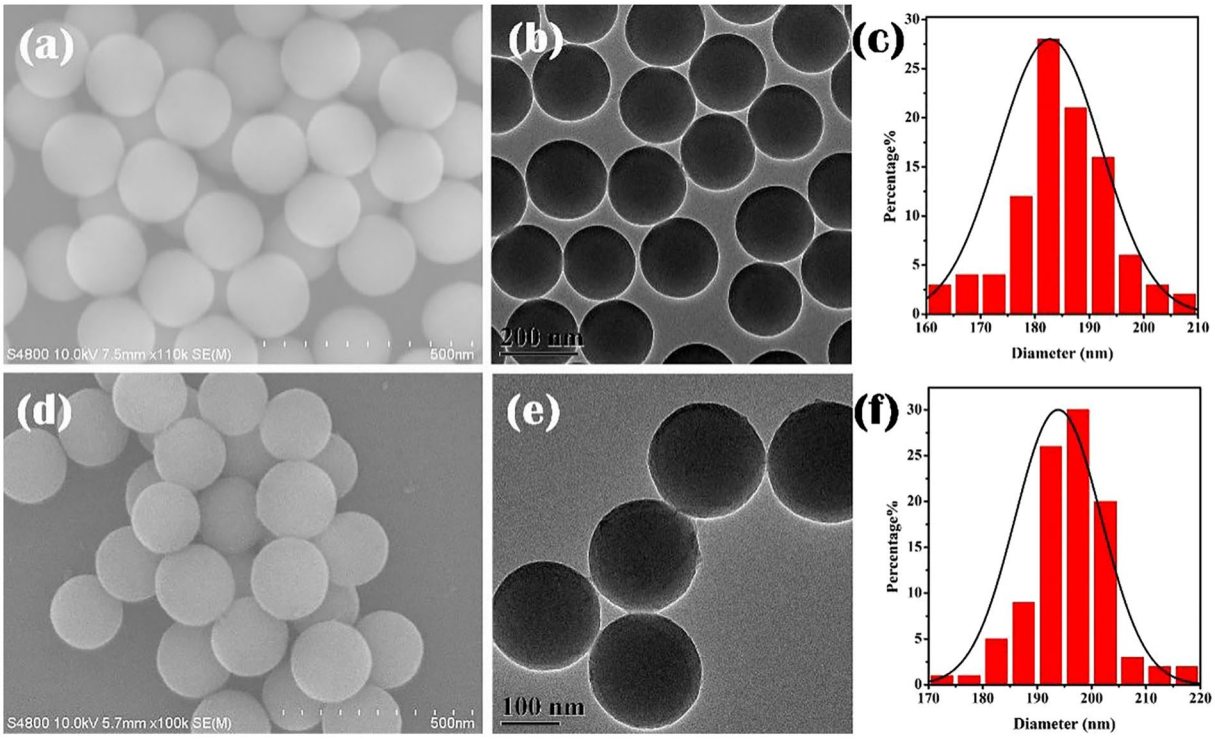

Figure 1. SEM and TEM images of SiO_2 (**a,b**) and SiO_2@AIPA-S-Si (**d,e**). Size distribution of SiO_2 (**c**) and SiO_2@AIPA-S-Si (**f**).

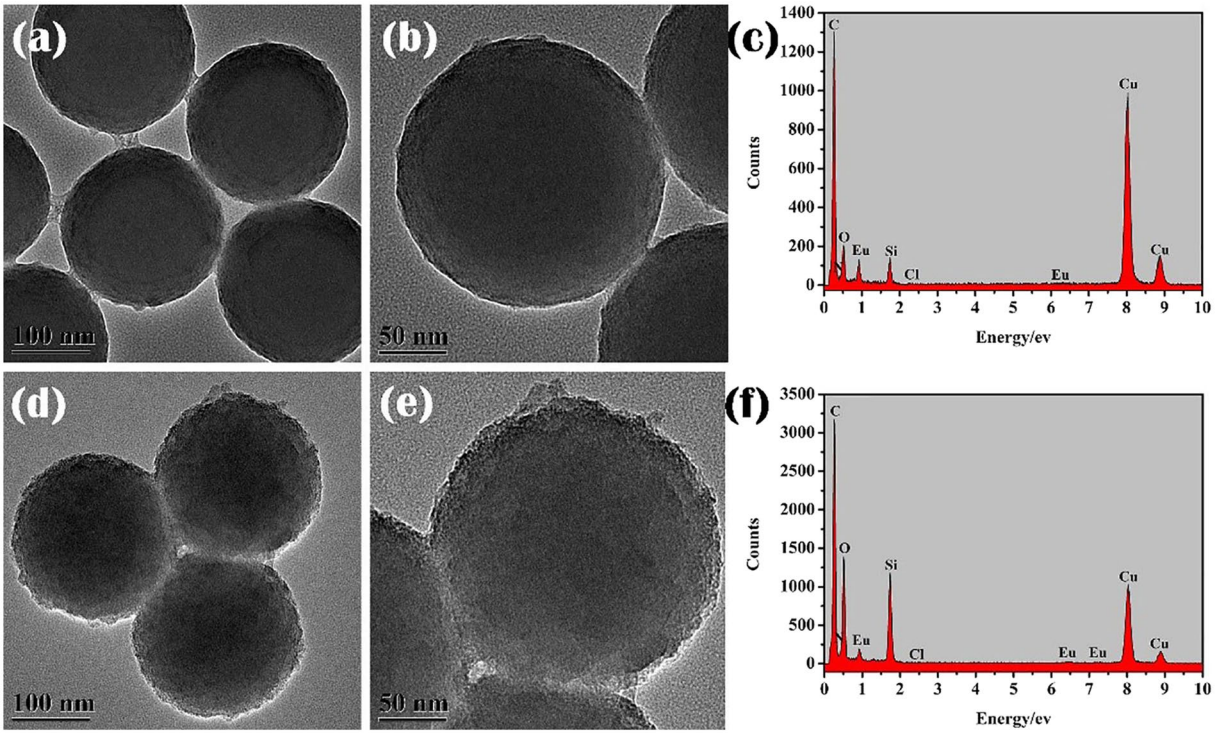

Figure 2. TEM images of SiO_2@AIPA-S-Si-Eu (**a,b**) and SiO_2@AIPA-S-Si-Eu@SiO_2 (**d,e**). EDX images of SiO_2@AIPA-S-Si-Eu (**c**) and SiO_2@AIPA-S-Si-Eu@SiO_2 (**f**).

(Fig. S4b) was located at 1635 cm^{-1} ($\nu_{C=O}$) and 1566 cm^{-1} (δ_{NH}), which was attributed to the stretching vibration of amide groups (–CONH–). The characteristic bands located at 1697 cm^{-1} belonged to stretching vibration of –C=O– (COOH). This further indicates that the ligand AIPA-S-Si was successfully coated on the surface of

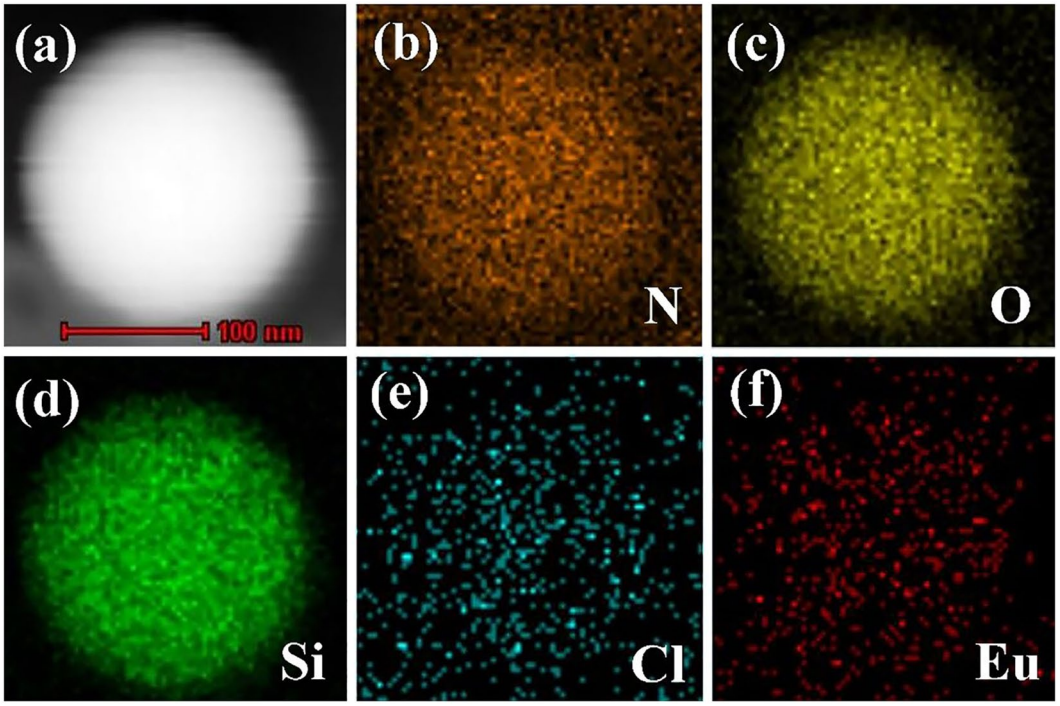

Figure 3. (**a**) HRTEM image of SiO_2@AIPA-S-Si-Eu@SiO_2 nanocomposite and corresponding elemental mapping images represent the (**b**) nitrogen mapping, (**c**) theoxygen mapping, (**d**) silicon mapping, (**e**) chlorinum mapping, and (**f**) europium mapping.

the SiO_2 microspheres. In the FT-IR spectrum of SiO_2@AIPA-S-Si-Eu (Fig. S4c), the characteristic absorption bands of –CONH– were located at 1627 cm^{-1} and 1558 cm^{-1}, respectively. Obviously, compared with SiO_2@AIPA-S-Si (Fig. S4b), the absorption band of amide groups was red shifted by 8 cm^{-1}, indicating that the first ligand AIPA-S-Si coordinated with the Eu^{3+} ions by carboxyl oxygen atom. Fig. S4d shows the FT-IR spectrum of SiO_2@AIPA-S-Si-Eu@SiO_2. After coating a layer of amorphous SiO_2 on the core-shell structured nanocomposite, the characteristic absorption band of SiO_2 appeared at 1095 cm^{-1} ($\nu_{Si\text{-}O\text{-}Si}$) and 952 cm^{-1} ($\nu_{Si\text{-}OH}$), and the absorption bands of –CONH– and –C=O– (COOH) were obviously weakened. This further confirmed the synthesis of the SiO_2@AIPA-S-Si-Eu@SiO_2 nanocomposite.

The FT-IR spectra analysis of SiO_2@AIPA-S-Si-Eu-phen and SiO_2@AIPA-S-Si-Eu-phen@SiO_2. The FT-IR spectra of SiO_2, phen, SiO_2@AIPA-S-Si-Eu-phen and SiO_2@AIPA-S-Si-Eu-phen@SiO_2 were shown in Fig. S5. In the FT-IR spectrum for phen (Fig. S5b), the stretching vibration of –C=N– appeared at 1589 cm^{-1}, and the bending vibration of C-H appeared at 740 cm^{-1} and 856 cm^{-1} [35,36]. In the FT-IR spectrum for SiO_2@AIPA-S-Si-Eu-phen (Fig. S5c), the corresponding characteristic absorption bands are red shifted to 1566 cm^{-1}($\nu_{C=N}$), 725 and 848 cm^{-1}($\delta_{C\text{-}H}$), respectively. The above results demonstrate the success of the coordination of the Eu^{3+} ions with the nitrogen atoms in the second ligand phen. As can be observed in the FT-IR spectrum of SiO_2@AIPA-S-Si-Eu-phen@SiO_2 nanocomposite (Fig. S5d), the absorption band of –C=N– is significantly weakened and the characteristic absorption band of SiO_2 appears in 1095 cm^{-1} ($\nu_{Si\text{-}O\text{-}Si}$) and 950 cm^{-1} ($\nu_{Si\text{-}OH}$), which further demonstrated that amorphous SiO_2 is successfully coated on the surface of core-shell structured nanocomposite.

XRD analysis. In order to study the structure of nanocomposites, the x-ray diffraction (XRD) patterns of all samples were tested from 5° to 80° at room temperature. As shown in Fig. S6, all samples exhibited similar wide diffraction peak at approximately 23° without any shift, except for a slight difference in intensity. The wide diffraction peak belongs to the amorphous SiO_2 [37,38]. The SiO_2@AIPA-S-Si (Fig. S6 (A,B)b) was the same as the pure SiO_2 (Fig. S6 (A,B)a) peak shape at about 23°, indicating that the first ligand (AIPA-S-Si) was grafted on the SiO_2 surface without changing the structure of the SiO_2. The peak shape of the core-shell structured nanocomposites SiO_2@AIPA-S-Si-Eu (Fig. S6Ac) and SiO_2@AIPA-S-Si-Eu-phen (Fig. S6Bc) were different from SiO_2@AIPA-S-Si. It was noticed that a new diffraction peak appears at about 10°, which may be attributed to the formation of the Eu complex. Fig. S6Bc indicates that SiO_2@AIPA-S-Si-Eu-phen nanocomposite shows some small diffraction peaks at 5–30°, while the diffraction peaks of amorphous SiO_2 at about 23° were significantly weakened, further indicating that the rare earth complexes coated on the surface of SiO_2 microspheres. Moreover, the peak shape of the core-shell-shell structured nanocomposites SiO_2@AIPA-S-Si-Eu@SiO_2 (Fig. S6Ad) and SiO_2@AIPA-S-Si-Eu-phen@SiO_2 (Fig. S6Bd) are similar to the pure SiO_2 peak shape, indicating that amorphous SiO_2 was successfully coated on the surface of the core-shell structured nanocomposite.

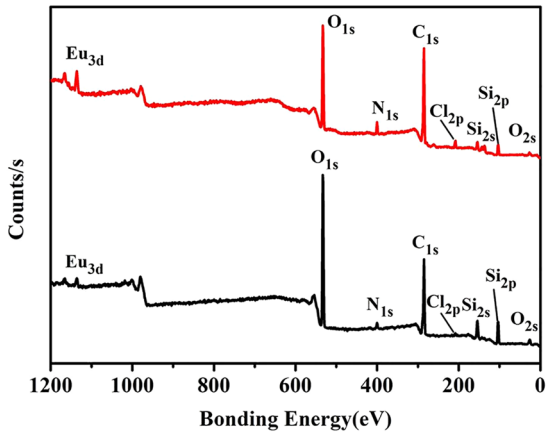

Figure 4. The XPS survey spectra of SiO_2@AIPA-S-Si-Eu (**a**) and SiO_2@AIPA-S-Si-Eu-phen (**b**).

TG analysis. In order to investigate core-shell and core-shell-shell structured nanocomposites have good thermal stability. The thermogravimetric analysis (TGA) curves of the core-shell and core-shell-shell structured nanocomposites were performed from 30 °C to 950 °C at a rate of 20 °C/min under N_2 atmosphere. The thermogravimetric curve of core-shell structured SiO_2@AIPA-S-Si-Eu-phen (a) and core-shell-shell structured SiO_2@AIPA-S-Si-Eu-phen@SiO_2 (b) were shown in Fig. S7. It can be observed that two nanocomposites have similar trends in weight loss and there were two major degradation steps. The first stage exhibited a weight loss of 3% and 6% for core-shell and core-shell-shell structured nanocomposites, respectively, which were attributed to the loss of water molecules physically adsorbed on the surface of the nanocomposites[39]. In the second stage, the weight loss of core-shell and core-shell-shell structured nanocomposites were 28% and 12%, respectively, which were due to the decomposition of organic complex. In general, the total weight loss percentage of core-shell and core-shell-shell structured nanocomposites were 31% and 18% from 34 °C to 670 °C. It was indicated that the percentage of organic complex in the core-shell structured nanocomposite is higher than that of the core-shell-shell structured nanocomposite, which further proves that amorphous SiO_2 was coated on the surface of the core-shell structured nanocomposite. In addition, the second stage organic complex of the core-shell and core-shell-shell structured nanocomposites began to decompose at temperatures of 125 °C and 161 °C, respectively. The result indicates that the decomposition temperature of the core-shell-shell structured nanocomposite is higher than the core-shell structured nanocomposite. Therefore, the thermal stability of the core-shell-shell structured nanocomposite is higher than that of the core-shell structured nanocomposite. At the same time, because the core-shell-shell structured nanocomposite has the protection of SiO_2 shell, it has a good promotion effect on thermal stability of nanocomposite.

XPS analysis. The surface chemical compositions of the core-shell structured nanocomposites SiO_2@AIPA-S-Si-Eu and SiO_2@AIPA-S-Si-Eu-phen were further confirmed by XPS testing. The survey scan ranging from 0 to 1200 eV was shown in Fig. 4, the results demonstrated that core-shell structured nanocomposites were mainly composed by the elements, including C, N, O,Si, Cl and Eu. As shown in the XPS spectra (Fig. S8) of core-shell structured nanocomposites, the binding energy of C (1 s, 284.78 eV), (1 s, 288.65 eV); N (1 s, 399.3 eV); O (1 s, 532.45 eV); Si (2p, 103.35 eV); Cl ($2p_{1/2}$, 209.25 eV), ($2p_{3/2}$, 207.65 eV) and Eu ($3d_{5/2}$, 1135.65 eV), ($3d_{3/2}$, 1165.75 eV) can be clearly seen, respectively[40–43]. However, since XPS is a technique for surface detection and its detection depth is less than 10 nm, the presence of an element of N, O, Si, Cl and Eu indicates that the Eu complex was coated on the surface of the silica microspheres[44]. The above data further indicates that the core-shell structured nanocomposites SiO_2@AIPA-S-Si-Eu and SiO_2@AIPA-S-Si-Eu-phen have been successfully synthesized.

Solid state luminescence properties. The excitation and emission spectra of the core-shell and core-shell-shell structured nanocomposites were measured in solid state by FLS-980 luminescence spectrometer at room temperature. The slit width of the nanocomposites SiO_2@AIPA-S-Si-Eu, SiO_2@AIPA-S-Si-Eu-phen, SiO_2@AIPA-S-Si-Eu@SiO_2 and SiO_2@AIPA-S-Si-Eu-phen@SiO_2 were 1, 0.7, 1, and 0.7 nm respectively. The luminescence intensity comparison of the core-shell and core-shell-shell structured nanocomposites were shown in Fig. 5. All nanocomposites exhibit similar luminescence spectra except for changes in intensity. The excitation spectra of all nanocomposites were recorded by monitoring at emission wavelength of 615 nm. The spectra were dominated by a broad excitation band centered at about 270–370 nm in ultraviolet region. It was designated as ligands that are absorbed into their $\pi \rightarrow \pi^*$ transitions[37]. As shown in Fig. 5, five characteristic emission peaks were observed at 579 nm, 591 nm, 615 nm, 652 nm and 701 nm which represented $^5D_0 \rightarrow {}^7F_J$ (J = 0, 1, 2, 3, 4) transitions of Eu^{3+} ions within $4f^6$ configuration, respectively. The strongest emission peak at 615 nm was attributed to the $^5D_0 \rightarrow {}^7F_2$ electrical dipole transition of Eu^{3+} ion, which was caused by the lack of inversion symmetry at Eu^{3+} ions site[45,46]. So, the strong red luminescence can be observed in the emisssion spectra. It can be seen from Fig. 5a that the luminescence intensities of core-shell structured nanocomposite SiO_2@AIPA-S-Si-Eu was 1397610 a.u. Figure 5b shows that the luminescence intensity of the core-shell structured nanocomposite SiO_2@AIPA-S-Si-Eu-phen was 2072052 a.u., which was 1.48 times higher than that of the core-shell structured

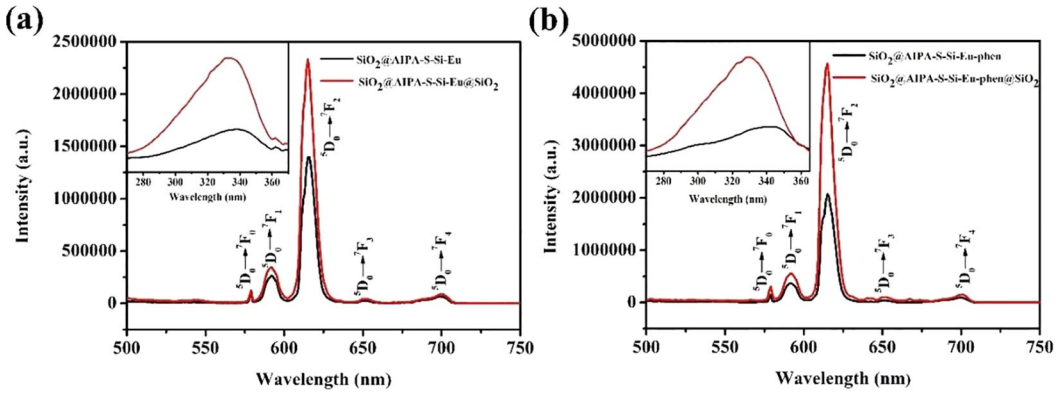

Figure 5. Emission spectra of (**a**) SiO_2@AIPA-S-Si-Eu (black) and SiO_2@AIPA-S-Si-Eu@SiO_2 (red), (**b**) SiO_2@AIPA-S-Si-Eu-phen (black) and SiO_2@AIPA-S-Si-Eu-phen@SiO_2 (red). Inset shows the corresponding Excitation spectra.

nanocomposite	Slit width (nm)	λ_{Ex} (nm)	λ_{Em} (nm)	I (a. u.)	Intensity Changes
SiO_2@AIPA-S-Si-Eu	1	339	615	1,397,610	
SiO_2@AIPA-S-Si-Eu@SiO_2	1	322	615	2,331,890	1.67
SiO_2@AIPA-S-Si-Eu-phen	0.7	340	615	2,072,052	
SiO_2@AIPA-S-Si-Eu-phen@SiO_2	0.7	328	615	4,571,858	2.21

Table 1. Luminescence emission spectra data of core-shell and core-shell-shell nanocomposites.

nanocomposite SiO_2@AIPA-S-Si-Eu. This is due to the addition of the second ligand (phen) can coordinate with the Eu^{3+} ion and improve the energy transfer efficiency, so that the nanocomposite luminescence intensity was significantly improved. On the other hand, the luminescence intensity of the core-shell-shell structured nanocomposite was stronger than that of the corresponding core-shell structured nanocomposite. From the data in Table 1, it was indicated that the two core-shell-shell structured nanocomposites increase by 1.67 times and 2.21 times compared with the corresponding core-shell structured nanocomposites, respectively. Since the core-shell structured nanocomposites were coated with a silica shell, which the high vibration energies loss of the ligand molecules (AIPA-S-Si, phen) or other quenching sites located at the surface of the core-shell structured nanocomposite could largely reduce. The silica shell can protect the rare earth complexes from quenching by the external environment[21]. Thus, the luminous intensity of the core-shell-shell structured nanocomposite is stronger than that of the corresponding core-shell structured nanocomposite. Luminescence intensity comparison data for all nanocomposites were shown in Table 1.

Aqueous solution luminescence properties. In order to further research the potential application of core-shell-shell structured nanocomposites in the biological field, we have tested the stability of core-shell-shell structured nanocomposites in aqueous solution. The core-shell-shell structured nanocomposites were dissolved in distilled water to prepare a suspension having a concentration of 0.1 g/L. The prepared solution was placed for 0 h, 24 h, 48 h and the luminescence intensity was measured. Figure 6 shows that the luminescence intensity of the nanocomposites in the aqueous still has strong luminescence intensity and no significant change after being placed for different time. Therefore, the core-shell-shell structured nanocomposites have excellent luminescence stability in aqueous solution.

Fig. S9 shows the calculated CIE chromaticity coordinates of all nanocomposites investigated. SiO_2@AIPA-S-Si-Eu, SiO_2@AIPA-S-Si-Eu@SiO_2, SiO_2@AIPA-S-Si-Eu-phen and SiO_2@AIPA-S-Si-Eu-phen@SiO_2 show a red emission located at (0.5152, 0.2655), (0.4893, 0.2536), (0.5736, 0.3124) and (0.5917, 0.3212) respectively. The results of chromaticity coordinates show that all the nanocomposites are located in the red or pink region.

Figure 7 exhibits, as an example, the red light image of SiO_2@AIPA-S-Si-Eu@SiO_2 (a,b) and SiO_2@AIPA-S-Si-Eu-phen@SiO_2 (e,f) nanocomposites without and under UV irradiation. In addition, the image also show the pink light image of a solution of SiO_2@AIPA-S-Si-Eu@SiO_2 (c,d) and SiO_2@AIPA-S-Si-Eu-phen@SiO_2 (g,h) nanocomposites dispersed in water without and under UV irradiation. Under ultraviolet irradiation, core-shell-shell structured nanocomposites exhibit bright red or pink light in solid or aqueous solution, which indicates that core-shell-shell structured nanocomposites have excellent luminous properties.

The luminescence lifetime. To further study the luminescence properties, the lifetime curve of nanocomposites was also measured at room temperature. As shown in Fig. S10, all curves follow a double exponential fit (1)[38]:

$$I_{(t)} = I_0 + A_1 \exp(-t/t_1) + A_2 \exp(-t/t_2) \quad (1)$$

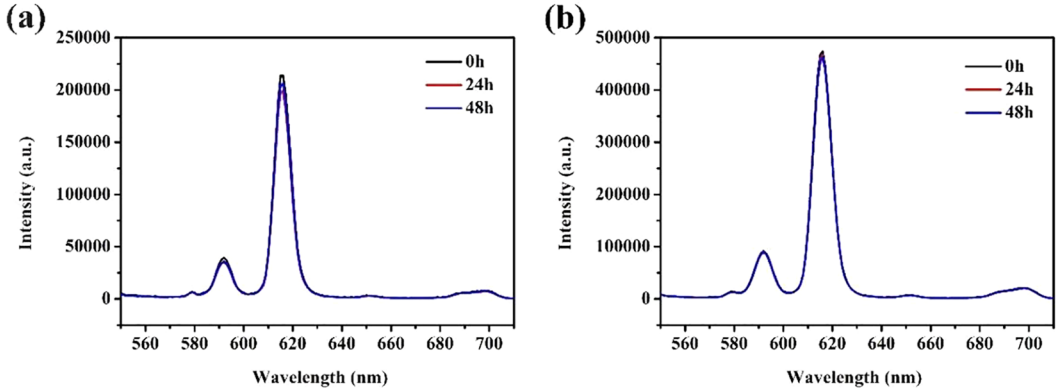

Figure 6. Emission spectra of (**a**) SiO_2@AIPA-S-Si-Eu@SiO_2 and (**b**) SiO_2@AIPA-S-Si-Eu-phen@SiO_2 after placement for 0 h, 24 h, 48 h in aqueous solution.

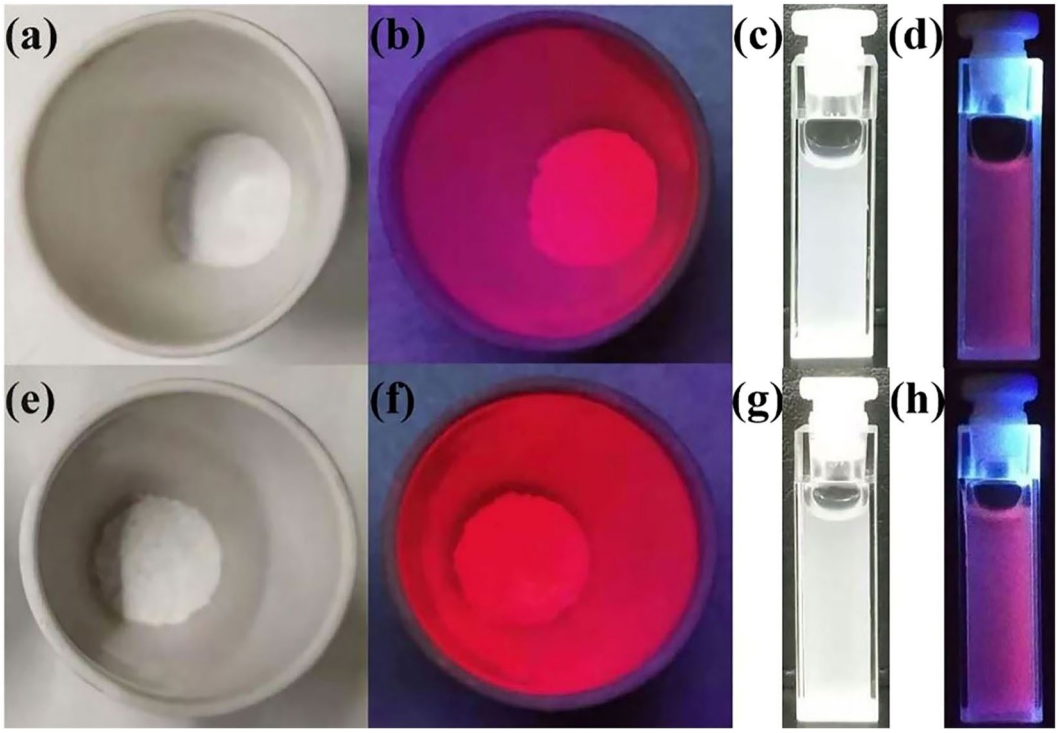

Figure 7. The images of SiO_2@AIPA-S-Si-Eu@SiO_2 (**a,b**) and SiO_2@AIPA-S-Si-Eu-phen@SiO_2 (**e,f**) without (**a,e**) and under UV irradiation (**b,f**). The images of SiO_2@AIPA-S-Si-Eu@SiO_2 (**c,d**) and SiO_2@AIPA-S-Si-Eu-phen@SiO_2 (**g,h**) dispersed in water without (**c,g**) and under UV irradiation (**d,h**).

where $I_{(t)}$ and I_0 are the luminescence intensities, A_1 and A_2 are the fitting parameters, and t_1 and t_2 are the decay time, respectively. In addcay lifetime (t) is calculated using Eq. (2):

$$t = (A_1t_1^2 + A_2t_2^2)/(A_1t_1 + A_2t_2) \quad (2)$$

Thus, the average liftime were detetmined to be 0.63, 1.10, 0.64, and 0.58 ms for the SiO_2@AIPA-S-Si-Eu, SiO_2@AIPA-S-Si-Eu@SiO_2, SiO_2@AIPA-S-Si-Eu-phen and SiO_2@AIPA-S-Si-Eu-phen@SiO_2. It can be found that all nanocomposites have a long lifetime.

Low temperature phosphorescence spectra. To further explain the luminescence mechanism of the nanocomposites. The low phosphorescence spectra of the ligands were tested on a FLS-980 phosphorescence spectrometer at 77 K. The excitation wavelengths of the ligands AIPA-S-Si and phen were 355 nm and 372 nm, respectively. The corresponding slit width was 1 nm and 10 nm, respectively. The triplet energy level of the ligand was determined by the half width of the band. In the phosphorescence spectra of the first ligand AIPA-S-Si (Fig. S11a), there was an emission band of 455 nm to 530 nm, indicating that the triplet energy level was 21978 cm^{-1} to 18868 cm^{-1}. The excited state energy level $^5D_0$ of Eu^{3+} ion was calculated to be 17277 cm^{-1}.

Therefore, the triplet energy level of the first ligand AIPA-S-Si was higher than the excitable energy level of the Eu^{3+} ion, and the ligand can effectively transfer the energy absorbed from the ultraviolet region to the central Eu^{3+} ions, thereby sensitizing the luminescence of the Eu^{3+} ion. In the phosphorescence spectrum of the second ligand phen, the emission band from 503 nm to 618 nm can be observed from the Fig. S11b. The corresponding triplet energy level was 19881 cm^{-1} to 16181 cm^{-1}. The highest triplet energy level of phen was also higher than the excitable energy level of Eu^{3+} ions, so the luminescence of Eu^{3+} ions can also be sensitized. The schematic diagram of the triplet energy levels and Eu^{3+} ions excited state levels of the ligands AIPA-S-Si and phen was shown in Fig. S12. Since the first ligand AIPA-S-Si and the second ligand phen can synergistically sensitize the Eu^{3+} ions. Therefore, the luminescence intensity of the SiO_2@AIPA-S-Si-Eu-phen nanocomposite was superior to that of the SiO_2@AIPA-S-Si-Eu nanocomposite. In summary, the presence of the ligands AIPA-S-Si and phen can sensitize Eu^{3+} ions to have excellent luminescent properties.

Conclusions

The four novel nanocomposites SiO_2@AIPA-S-Si-Eu, SiO_2@AIPA-S-Si-Eu-phen, SiO_2@AIPA-S-Si-Eu@SiO_2 and SiO_2@AIPA-S-Si-Eu-phen@SiO_2 have been successfully prepared; All nanocomposites have excellent luminescence properties, and the core-shell-shell structured nanocomposites have stronger luminescence intensity than the corresponding core-shell structured nanocomposites; The aqueous solution of core-shell-shell structured nanocomposites have excellent luminescence stability, and the luminescence intensity is almost unchanged after being placed for 0 h, 24 h and 48 h at room temperature; Besides, the core-shell and core-shell-shell structured nanocomposites can also save rare earth resources and reduce production cost in the actual production process; More importantly, the silanol groups on the surface of the core-shell-shell structured nanocomposites are easily attached to biomolecule. Consequently, the research of core-shell-shell structured nanocomposites not only has potential applications in biology, but also excellent luminescent properties provide new research ideas for other luminescent materials.

Materials and Methods

Materials. 5-amino-iso-phthalic acid (AIPA, 99.8%, Aldrich), cetyltrimethylammonium bromide (CTAB), acetone (C_3H_4O, 99%), 3-(triethoxysilyl)-propyl isocyanate (TEPIC, 96%, Aldrich), Europium oxide (Eu_2O_3, 99.999%), perchloric acid ($HClO_4$, 1 mol/L), Europium perchlorate ($Eu(ClO_4)_3.nH_2O$) was prepared by Eu_2O_3 and $HClO_4$. Tetraethyl orthosilicate (TEOS, 99%), ammonia solution ($NH_3.H_2O$, 25%), 1,10-phenanthroline (phen, 99%), absolute ethanol (C_2H_5OH, 99%). All chemical reagents are of analytical grade.

Synthesis of ligand (AIPA-S-Si). First, 2 mmol 5-aminoisophthalic acid (AIPA) was placed in a 100 mL dry three-neck flask, and 40 mL acetone was added to completely dissolve it. Then, 6 mmol 3-(triethoxysilyl)-propyl isocyanate (TEPIC) was added to the above solution, and reflux reaction was continued at 55 °C for 15 h to ensure complete reaction. It was clearly observed that a large amount of white precipitate was produced at the bottom of the flask. Subsequently, the remaining solvent was evaporated to dryness, washed three times with cold n-hexane. Finally, the product was dried at 60 °C for 5 h to give a white powder. The product is defined as AIPA-S-Si ($C_{18}H_{28}N_2O_8Si$, M = 428 g/mol). Yield: 80%. The elemental analysis results are as follows: C 50.36%, H 6.35%, N 6.61%; Found: C 50.47%, H 6.54%, N 6.54%. The ^1H NMR (DMSO as a solvent) data are as follows (Fig. S13): δ 13.13 (s, 2H, –COOH), δ 8.88 (s, 1H, –NH–), δ 8.22 (s, 1H, –CH–), δ 8.01 (s, 1H, CH–), δ 6.27 (t, 1H, –NH–), δ 3.76 (q, 6H, $–CH_2–$), δ 3.06 (q, 2H, $–CH_2–$), δ 1.5 (m, 2H, $–CH_2–$), δ 1.14 (t, 9H, $–CH_3$), δ 0.56 (t, 2H, $–CH_2–$).

Synthesis of SiO_2 microspheres. The SiO_2 microspheres were prepared according to the Stöber method[47]. Specifically, 1.7 mL ammonia water and 4 mL distilled water were added to 35 mL absolute ethanol, and then 1.7 mL TEOS was added dropwise to the above solution under magnetic stirring. Then, a white suspension was obtained after continuing the reaction for 6 h at room temperature. The resulting product was centrifuged, washed with ethanol and distilled water several times, respectively. Finally, SiO_2 microspheres were dried at 50 °C for 5 h.

Synthesis of SiO_2@AIPA-S-Si. Briefly, 0.1 g as-prepared SiO_2 microspheres were accurately weighed and dissolved in a mixed solution of 10 mL absolute ethanol and 10 mL distilled water, and then the as-prepared ligand (AIPA-S-Si) was ultrasonically dissolved in 20 mL 1,4-dioxane. Subsequently, the ligand (AIPA-S-Si) solution was gradually added dropwise to the silica solution, and the reaction was stirred at room temperature for 36 h. The product was washed three times with absolute ethanol and collected by centrifugation at 8000 r. min^{-1}. Finally, the product was dried at 50 °C for 10 h. The product is defined as SiO_2@AIPA-S-Si.

Synthesis of SiO_2@AIPA-S-Si-Eu and SiO_2@AIPA-S-Si-Eu@SiO_2. Typically, 0.0550 g as-prepared SiO_2@AIPA-S-Si was uniformly dispersed in 15 mL absolute ethanol. Subsequently, 0.0550 g $Eu(ClO_4)_3.nH_2O$ was dissolved in 5 mL absolute ethanol, which was added dropwise to the above solution, and fully reacted under magnetic stirring at 50 °C for 24 h. The obtained product was centrifuged, washed with absolute ethanol several times, and the white product was dried at 50 °C for 5 h. The product is defined as SiO_2@AIPA-S-Si-Eu.

0.02 g SiO_2@AIPA-S-Si-Eu and 0.01 g CTAB were dissolved in 20 mL of a mixed solvent (5 mL distilled water, 15 mL ethanol), then add the appropriate amount of ammonia water and 15 μL TEOS. Then, the mixture was continuously stirred at room temperature for 24 h. The resulting suspension was washed six times with ethanol and water. After centrifugation at 8000 r.min^{-1}, the final product was dried at 50 °C for 5 h. The product is defined as SiO_2@AIPA-S-Si-Eu@SiO_2.

Synthesis of SiO_2@AIPA-S-Si-Eu-phen and SiO_2@AIPA-S-Si-Eu-phen@SiO_2. The synthesis method was identical to the above method. 0.05 g SiO_2@AIPA-S-Si-Eu and 0.04 g phen were ultrasonically dispersed in 15 mL absolute ethanol, 0.7 g $Eu(ClO_4)_3.nH_2O$ was dissolved in 5 mL absolute ethanol, and then slowly dropped into the above solution. The reaction was carried out under magnetic stirring at 50 °C for 24 h. The white powder obtained after centrifugation, washing and drying was defined as SiO_2@AIPA-S-Si-Eu-phen. Correspondingly, the core-shell-shell structured nanocomposite was synthesized in the same method as above, and the obtained product is defined as SiO_2@AIPA-S-Si-Eu-phen@SiO_2.

Characterization. ^1H nuclear magnetic resonance (NMR) spectrum was recorded on a Bruker Advancell spectrometer with DMSO as the solvent. All samples were analyzed by FT-IR spectroscopy, which were measured by a Bruker VERTEX70 FT-IR spectrophotometer in the wave number range of 400–4000 cm^{-1} using potassium bromide (KBr) pellets. The X-ray diffraction (XRD) analysis was recorded using a PANalytical Empyrean diffractometer, which equipped with Cu Kalpha1 radiation (1.5405 Å), the scanning rate was 15°/min in the 2θ range of 5–80° at room temperature. The morphology of the nanocomposites was characterized on Hitachi S-4800 scanning electron microscopy (SEM) at 20 kV and FEI Tecnai F20 transmission electron microscopy (TEM) at an acceleration voltage of 200 kV. Thermogravimetric analysis (TGA) was tested on a STA6000 thermogravimetric analyzer in air at a heating rate of 20 °C/min from room temperature to 950 °C. Luminescence spectra were tested at room temperature using a FLS-980 (Edinburgh Instruments, England) with a xenon lamp as the light source. Phosphorescence spectra were measured at 355 nm and 372 nm excitation on a FLS-980 spectrofluorometer at 77 K. X-ray photoelectron spectroscopy (XPS) spectra were recorded on Thermo ESCALAB 250Xi spectrometer (Thermo Fisher Scientific, Waltham, MA, USA).

Received: 18 October 2019; Accepted: 7 February 2020;
Published online: 26 February 2020

References

1. Gawande, M. B. *et al*. Core-shell nanoparticles: synthesis and applications in catalysis and electrocatalysis. *Chem. Soc. Rev.* **44**, 7540–7590, https://doi.org/10.1039/c5cs00343a (2015).
2. Li, B. M. *et al*. Coordination polymer core/shell structures: Preparation and up/downconversion luminescence. *J. Colloid Interface Sci.* **479**, 15–19, https://doi.org/10.1016/j.jcis.2016.06.038 (2016).
3. Yu, J. B. *et al*. Efficient Electroluminescence from New Lanthanide (Eu^{3+}, Sm^{3+}) Complexes. *Inorg. Chem.* **44**, 1611–1618, https://doi.org/10.1021/ic0485561 (2005).
4. Li, L. *et al*. Preparation of core/shell structured silicate composite filler and its reinforcing property. *Powder Technol.* **332**, 27–32, https://doi.org/10.1016/j.powtec.2018.03.037 (2018).
5. Su, L. W., Jing, Y. & Zhou, Z. Li ion battery materials with core-shell nanostructures. *Nanoscale.* **3**, 3967–3983, https://doi.org/10.1039/c1nr10550g (2011).
6. Liu, G. F. *et al*. One pot synthesis and optimized luminescent intensity of $Gd_2(WO_4)_3$: Yb^{3+}/Ho^{3+}@SiO_2 nanoparticles for biological application. *J. Lumin.* **206**, 1–5, https://doi.org/10.1016/j.jlumin.2018.10.039 (2019).
7. Lei, Z. W. *et al*. Can plasmon suppress the concentration quenching of Eu^{3+} in Au/SiO_2/Y_2O_3:Eu^{3+} nanoparticles? *J. Lumin.* **206**, 359–363, https://doi.org/10.1016/j.jlumin.2018.10.052 (2019).
8. Yu, X. G., Wan, J. Q., Shan, Y., Chen, K. Z. & Han, X. D. A Facile Approach to Fabrication of Bifunctional Magnetic-Optical Fe_3O_4@ZnS Microspheres. *Chem. Mater.* **21**, 4892–4898, https://doi.org/10.1021/cm902667b (2009).
9. Suresh, C. *et al*. SiO_2@LaOF:Eu^{3+} core-shell functional nanomaterials for sensitive visualization of latent fingerprints and WLED applications. *J.Colloid Interface Sci.* **518**, 200–215, https://doi.org/10.1016/j.jcis.2018.01.093 (2018).
10. Liu, S. Q., Zhang, N., Tang, Z. R. & Xu, Y. J. Synthesis of One-Dimensional CdS@TiO_2 Core-Shell Nanocomposites Photocatalyst for Selective Redox: The Dual Role of TiO_2 Shell. *ACS Appl. Mater. Interfaces.* **4**, 6378–6385, https://doi.org/10.1021/am302074p (2012).
11. Guerrero-Martínez, A., Pérez-Juste, J. & Liz-Marzán, L. M. Recent Progress on Silica Coating of Nanoparticles and Related Nanomaterials. *Adv. Mater.* **22**, 1182–1195, https://doi.org/10.1002/adma.200901263 (2010).
12. Kang, X. J. *et al*. Core-Shell Structured Up-Conversion Luminescent and Mesoporous $NaYF_4$:Yb^{3+}/Er^{3+}@nSiO_2@mSiO_2 Nanospheres as Carriers for Drug Delivery. *J. Phys. Chem. C* **115**, 15801–15811, https://doi.org/10.1021/jp203039t (2011).
13. Liu, C. & Yan, B. Highly effective chemosensor of a luminescent silica@lanthanide complex@MOF heterostructured composite for metal ion sensing. *RSC Adv.* **5**, 101982–101988, https://doi.org/10.1039/C5RA19973E (2015).
14. Yang, L. *et al*. Luminescent SiO_2@Tb/guanosine 5′-monophosphate core-shell nanoscale coordination polymers for superoxide anion detection. *Talanta.* **191**, 74–80, https://doi.org/10.1016/j.talanta.2018.08.041 (2019).
15. Alexey, P. *et al*. Synthesis and Characterization of Monodisperse Metallodielectric SiO_2@Pt@SiO_2 Core-Shell-Shell Particles. *Langmuir.* **32**, 848–857, https://doi.org/10.1021/acs.langmuir.5b03631 (2016).
16. Ma, Y. Y. *et al*. Preparation, characterization and luminescence properties of core-shell ternary terbium composites SiO_2(600)@Tb(MABA-Si).L. *R. Soc. open sci.* **5**, 171655, https://doi.org/10.1098/rsos.171655 (2018).
17. Gao, J. F. *et al*. Synthesis and fluorescence properties of CdTe:Eu^{3+} nanocrystals and core-shell SiO_2-coated CdTe:Eu^{3+} nanospheres. *Rare Met.* **3**, 989–995, https://doi.org/10.1007/s12598-018-1180-1 (2019).
18. Yang, K. S. *et al*. Controlled synthesis of $EuPO_4$ nano/microstructures and core-shell SiO_2@$EuPO_4$ nanostructures with improved photoluminescence. *RSC Adv.* **7**, 52238–52244, https://doi.org/10.1039/C7RA10556H (2017).
19. Qin, C. X., Qin, L., Chen, G. Q., Xu, H. T. & Lin, T. Preparation and luminescence properties of SiO_2@$LaBO_3$:Eu^{3+} nanoparticles. *J. Nanopart. Res.* **15**, 1827, https://doi.org/10.1007/s11051-013-1827-7 (2013).
20. Chen, K. X., Kang, M., Liu, M., Shen, S. M. & Sun, R. Synthesis of di-functional ligand and fluorescently labeling SiO_2 microspheres. *Opt. Mater.* **79**, 464–469, https://doi.org/10.1016/j.optmat.2018.04.019 (2018).
21. Feng, L. N. *et al*. Synthesis and Luminescence Properties of Core-Shell-Shell Composites: SiO_2@PMDA-Si-Tb@SiO_2 and SiO_2@PMDA-Si-Tb-phen@SiO_2. *Nanomaterials* **9**, 189, https://doi.org/10.3390/nano9020189 (2019).
22. Fu, Z. F. *et al*. Synthesis, characterization and luminescence of europium perchlorate with MABA-Si complex and coating structure SiO_2@Eu(MABA-Si) luminescence nanoparticles. *Luminescence* **32**, 327–333, https://doi.org/10.1002/bio.3182 (2017).
23. Li, W. X. *et al*. Preparation, characterization, and luminescence properties of dysprosium perchlorate with MABA-Si and phen or dipy complexes as well as SiO_2@Dy(MABA-Si)L core-shell structure nanometermeter luminescent composites. *J. Lumin.* **178**, 470–478, https://doi.org/10.1016/j.jlumin.2016.06.019 (2016).
24. Aldalbahi, A., Rahaman, M. & Ansari, A. A. Mesoporous silica modified luminescent Gd_2O_3:Eu nanoparticles:physicochemical and luminescence properties. *J. Sol-Gel Sci. Technol.* **89**, 785–795, https://doi.org/10.1007/s10971-018-4897-2 (2019).

25. Li, G. Z. *et al*. Synthesis and photoluminescence of core-shell structured spherical SiO_2@YPO_4:Tb^{3+} phosphors via sol-gel process. *J. Lumin.* **132**, 2961–2967, https://doi.org/10.1016/j.jlumin.2012.06.015 (2012).
26. Ansari, A. A. Photochemical studies of monodispersed YPO_4:Eu microspheres: The role of surface modification on structural and luminescence properties. *J. Photochem. Photobiol. A: Chem.* **343**, 126–132, https://doi.org/10.1016/j.jphotochem.2017.04.021 (2017).
27. Han, Y. H. & Lin, J. Luminescence and energy transfer of organically modified silica xerogels (OMSX) doped and undoped with Eu^{3+} and Tb^{3+}. *J. Solid State Chem.* **171**, 396–400, https://doi.org/10.1016/s0022-4596(02)00220-7 (2003).
28. Yan, B., Li, Y. Y. & Guo, L. Photofunctional ternary rare earth (Eu^{3+}, Tb^{3+}, and Sm^{3+}) hybrid xerogels with hexafluoroacetylacetonate derived building block and bis(2-methoxyethyl) ether through coordination bonds. *Inorg. Chem. Commun.* **14**, 910–912, https://doi.org/10.1016/j.inoche.2011.03.028 (2011).
29. Yan, B. & Wan, F. F. Molecular design and photo-physics of quaternary hybrid terbium centered systems with novel functional di-urea linkages of strong chemical bonds through hydrogen transfer addition. *J. Organomet. Chem.* **692**, 2395–2401, https://doi.org/10.1016/j.jorganchem.2007.02.025 (2007).
30. Mondal, A. N. *et al*. Novel silica-functionalized aminoisophthalic acid-based membranes for base recovery via diffusion dialysis. *J. Membr. Sci.* **507**, 90–98, https://doi.org/10.1016/j.memsci.2016.02.016 (2016).
31. Wang, F. F. & Yan, B. Intramolecular energy transfer and luminescence enhancement effect in inert rare earth ions (La, Y, Gd)-Eu^{3+} (Tb^{3+}) co-fabricated organic-inorganic hybrid materials by covalent grafting. *Photochem. Photobiol. A: Chem.* **194**, 238–246, https://doi.org/10.1016/j.jphotochem.2007.08.016 (2008).
32. Xu, X. L., Hu, F. & Shuai, Q. Click Chemistry-Assisted Synthesis of a β-D-Galactose-Targeted SiO_2@RC Shell-Core Structure as a Nanoplatform for Metal-Based Complex Delivery. *Inorg. Chem.* **57**, 10694–10701, https://doi.org/10.1021/acs.inorgchem.8b01335 (2018).
33. Jiu, H. F. *et al*. Synthesis, luminescent and drug-release properties of SiO_2@Y_2O_3:Eu hollow mesoporous microspheres. *J. Porous Mater.* **22**, 1511–1518, https://doi.org/10.1007/s10934-015-0033-7 (2015).
34. Alcaraz, L. & Isasi, J. Synthesis and study of $Y_{0.9}Ln_{0.1}VO_4$ nanophosphors and $Y_{0.9}Ln_{0.1}VO_4$@SiO_2 luminescent nanocomposites with Ln=Eu, Dy, Er. *Ceram. Int.* **43**, 5311–5318, https://doi.org/10.1016/j.ceramint.2017.01.069 (2017).
35. Li, W. X. *et al*. Fluorescence enhancement of samarium (III) perchlorate by 1,10-phenanthroline on Phenylnaphthoylmethyl sulfoxide complex and luminescence mechanism. *J. Lumin.* **143**, 746–753, https://doi.org/10.1016/j.jlumin.2012.06.038 (2013).
36. Tang, D. H., Zhang, W. T., Qiao, Z. N., Liu, Y. L. & Huo, Q. S. Functionalized mesoporous silica nanoparticles as a catalyst to synthesize a luminescent polymer/silica nanocomposite. *RSC Adv.* **6**, 16461–16466, https://doi.org/10.1039/C5RA25135D (2016).
37. Zhang, Q. *et al*. Novel organic-inorganic amorphous photoactive hybrid films with rare earth (Eu^{3+}, Tb^{3+}) covalently embedded into silicon-oxygen network via sol-gel process. *Mater. Res. Bull.* **70**, 379–384, https://doi.org/10.1016/j.materresbull.2015.04.057 (2015).
38. Chang, M. Q. *et al*. Photocatalytic and Photoluminescence Properties of Core-Shell SiO_2@TiO_2:Eu^{3+}, Sm^{3+} and Its Etching Products. *ACS Sustainable Chem. Eng.* **6**, 223–236, https://doi.org/10.1021/acssuschemeng.7b02285 (2018).
39. Zhang, Q., Sheng, Y., Zheng, K. Y. & Zou, H. F. New kinds of hybrid materials containing covalently bonded Tb^{3+} (Eu^{3+}) complexes organically modified titania and alumina network via sol-gel process. *J. Sol-Gel Sci. Technol.* **77**, 152–159, https://doi.org/10.1007/s10971-015-3839-5 (2016).
40. Bagheri, A., Arandiyan, H., Adnan, N. N. M., Boyer, C. & Lim, M. Controlled Direct Growth of Polymer Shell on Upconversion Nanoparticle Surface via Visible Light Regulated Polymerization. *Macromol.* **50**, 7137–7147, https://doi.org/10.1021/acs.macromol.7b01405 (2017).
41. Shutthanandan, V. *et al*. Applications of XPS in the characterization of Battery materials. *J. Electron. Spectrosc. Relat. Phenom.* **231**, 2–10, https://doi.org/10.1016/j.elspec.2018.05.005 (2019).
42. Li, G. L. *et al*. Hairy Hybrid Nanoparticles of Magnetic Core, Fluorescent Silica Shell, and Functional Polymer Brushes. *Macromol.* **42**, 8561–8565, https://doi.org/10.1021/ma901592j (2009).
43. Sheng, G. D., Dong, H. P., Shen, R. P. & Li, Y. M. Microscopic insights into the temperature-dependent adsorption of Eu(III) onto titanate nanotubes studied by FTIR, XPS, XAFS and batch technique. *Chem. Eng. J.* **217**, 486–494, https://doi.org/10.1016/j.cej.2012.10.076 (2013).
44. Zhang, X. R., Kong, X. H., Yuan, L. Y., Chai, Z. F. & Shi, W. Q. Coordination of Eu(III) with 1,10-Phenanthroline-2,9-dicarboxamide Derivatives: A Combined Study by MS, TRLIF, and DFT. *Inorg. Chem.* **58**, 10239–10247, https://doi.org/10.1021/acs.inorgchem.9b01400 (2019).
45. Babu, B. C., Wang, G. G., Baker, A. P. & Wang, B. L. Synthesis, photoluminescence, energy transfer and thermal stability of $SmPO_4$@SiO_2:Eu^{3+} core-shell structured red phosphors for WLEDs. *J. Alloys Compd.* **766**, 74–87, https://doi.org/10.1016/j.jallcom.2018.06.256 (2018).
46. Sheng, K., Yan, B., Qiao, X. F. & Guo, L. Rare earth (Eu/Tb)/phthalic acid functionalized inorganic Si-O/organic polymeric hybrids: Chemically bonded fabrication and photophysical property. *J. Photochem. Photobiol. A: Chem.* **210**, 36–43, https://doi.org/10.1016/j.jphotochem.2009.12.008 (2010).
47. Stöber, W. & Fink, A. Controlled Growth of Monodisperse Silica Spheres in the Micron Size Range. *J. Colloid Interf. Sci.* **26**, 62–69, https://doi.org/10.1016/0021-9797(68)90272-5 (1968).

Acknowledgements

This research was funded by the Major projects of Natural Science Foundations of Inner Mongolia Science Foundation (No. 2015ZD01), the Natural Science Foundations of Inner Mongolia Science Foundation (No. 2015MS0502) and the major basic research and open project of the Inner Mongolia Autonomous Region (30500-515330303).

Author contributions

W.X.L. and Y.Q. conceived the experiment; Y.Q. conducted the experiment. W.X.L. and Y.Q. analysed the experimental results. Y.Q. wrote the manuscript. W.X.L., Y.Q., Y.S.Z., J.R.B., L.N.F., Y.Y.M., K.S.Y., A.P.W., H.B., Y.J.Y., contributed to the scientific discussion of the results. All authors reviewed the manuscript.

Competing interests

The authors declare no competing interests.

Additional information

Supplementary information is available for this paper at https://doi.org/10.1038/s41598-020-60538-w.

Correspondence and requests for materials should be addressed to W.L.

Reprints and permissions information is available at www.nature.com/reprints.